Computational Approach for Ranking Mutant Enzymes According to Catalytic Reaction Rates

ARTICLE *in* THE JOURNAL OF PHYSICAL CHEMISTRY B · MARCH 2009

Impact Factor: 3.3 · DOI: 10.1021/jp810363k · Source: PubMed

4 AUTHORS, INCLUDING:

Alexander V. Soudackov
University of Illinois, Urbana-Champaign
54 PUBLICATIONS **1,753** CITATIONS

SEE PROFILE

Published in final edited form as:
J Phys Chem B. 2009 March 19; 113(11): 3579–3583. doi:10.1021/jp810363k.

Computational Approach for Ranking Mutant Enzymes According to Catalytic Reaction Rates

Malika Kumarasiri, **Gregory A. Baker**, **Alexander V. Soudackov**, and **Sharon Hammes-Schiffer**
Department of Chemistry, 104 Chemistry Building, Pennsylvania State University, University Park, PA 16802; shs@chem.psu.edu

Abstract

A computationally efficient approach for ranking mutant enzymes according to the catalytic reaction rates is presented. This procedure requires the generation and equilibration of the mutant structures, followed by the calculation of partial free energy curves using an empirical valence bond potential in conjunction with biased molecular dynamics simulations and umbrella integration. The individual steps are automated and optimized for computational efficiency. This approach is used to rank a series of 15 dihydrofolate reductase mutants according to the hydride transfer reaction rate. The agreement between the calculated and experimental changes in the free energy barrier upon mutation is encouraging. The computational approach predicts the correct direction of the change in free energy barrier for all mutants, and the correlation coefficient between the calculated and experimental data is 0.82. This general approach for ranking protein designs has implications for protein engineering and drug design.

I. Introduction

Computational protein design is a rapidly growing field with potential applications in pharmaceuticals, biotechnology, and other industrial processes. Since most protein design protocols generate large numbers of designs,[1–3] an efficient method for ranking these designs according to specified criteria is essential. This type of ranking process enables the selection of a smaller number of designs for experimental characterization. A variety of criteria could be used in this ranking process, including protein stability, substrate binding energy, and activity. Often the objective is to rank protein designs according to the enzyme-catalyzed reaction rate. Within the framework of transition state theory, the rate of a chemical reaction is exponentially related to the free energy barrier. In this case, the protein designs are ranked according to the relative free energy barriers of the chemical step of interest.

In this paper, we present a computational approach for ranking mutant enzymes according to the relative free energy barriers associated with the catalyzed chemical reaction. The mutant enzymes are generated using a rotamer library[4] in conjunction with restrained minimizations and molecular dynamics simulations. For each mutant, the partial free energy curve for the chemical step of interest is calculated along a collective reaction coordinate using biased molecular dynamics simulations and umbrella integration[5,6] with an empirical valence bond potential.[7,8] This procedure does not include any type of parameter fitting for the mutants. Each step in the procedure can be automated and optimized for the specific enzyme system.

We apply this ranking approach to dihydrofolate reductase (DHFR), which catalyzes the reduction of 7,8-dihydrofolate (DHF) into 5,6,7,8-tetrahydrofolate (THF) using the coenzyme

Correspondence to: Sharon Hammes-Schiffer.

nicotinamide adenine dinucleotide phosphate (NADPH).[9] In this reaction, the hydride is transferred from the NC4 position of the NADPH cofactor to the C6 position of the protonated dihydrofolate substrate. The product THF is essential for the synthesis of purines, pyrimidines, and certain amino acids. As a result, DHFR inhibition has been promoted as a pharmacological target for antibacterial agents and anticancer drugs.[10–14] Furthermore, the hydride transfer reaction catalyzed by DHFR and its mutants has been the subject of a wide variety of experimental[15–29] and theoretical[30–43] studies. In particular, kinetic measurements on 15 single mutant DHFR enzymes indicate hydride transfer rates ranging from 0.2 s^{-1} to 319 s^{-1} at pH ≈ 7.[16–21] The objective of this paper is to use the computational approach outlined above to rank these 15 DHFR mutant enzymes according to the rate of hydride transfer and compare the results to the available experimental data.

An outline of this paper is as follows. In Section II, we present the general computational ranking approach and describe its implementation for studying the hydride transfer reaction in DHFR. Section III compares the experimental and calculated changes in free energy barriers for this enzyme-catalyzed reaction. The conclusions are presented in Section IV.

II. Methods

In this paper, we calculate the free energy barrier for hydride transfer in wild-type (WT) DHFR and 15 mutants to determine the change in the free energy barrier upon mutation. These 15 mutants were identified from a general literature search for experimental measurements of the hydride transfer rate at pH ≈ 7.[44] The hydride transfer reaction catalyzed by DHFR is depicted in Figure 1. We studied this reaction previously in WT DHFR,[31,32,45] as well as a few selected mutants,[33,34] with a hybrid quantum-classical molecular dynamics approach, which includes the nuclear quantum effects of the transferring hydrogen with grid-based or path integral methods. Here we use the same simulation system and EVB potential but do not include the nuclear quantum effects for computational efficiency. Based on our previous calculations on DHFR mutants,[33,34] the decrease in the free energy barrier due to the inclusion of these nuclear quantum effects is expected to be similar for all mutants. Thus, the neglect of the nuclear quantum effects should not significantly impact the changes in the free energy barrier upon mutation or the associated qualitative ranking of the mutant enzymes.

In previous simulations, the initial coordinates were obtained from a crystal structure of *Escherichia coli* DHFR complexed with $NADP^+$ and folate (PDB code 1rx2).[22] In the present paper, we start with a snapshot of the equilibrated reactant state obtained from previous simulations.[32,45] The present simulation system includes the entire protein, the substrate, and the cofactor solvated by 4097 explicit water molecules in a truncated octahedral periodic box with a distance of 66.55 Å between opposing square faces. The potential energy surface of the hydride transfer is represented by a two-state empirical valence bond (EVB) potential,[7] where state 1 corresponds to the transferring hydrogen atom bonded to the donor carbon, and state 2 corresponds to the transferring hydrogen atom bonded to the acceptor carbon. The diagonal elements of the EVB Hamiltonian are based on the GROMOS force field[46] with the covalent bond involving the transferring hydrogen represented by a Morse potential.[31] The two constant EVB parameters corresponding to the relative energy of the two valence bond states and the coupling between these states are 65.25 kcal/mol and 34.66 kcal/mol and are fixed at these values for all mutants. These parameters were determined in Ref. 32 by fitting the results obtained from hybrid quantum/classical molecular dynamics simulations of WT DHFR to the experimental free energies of reaction and activation obtained from the pH-independent forward and reverse hydride transfer reaction rate constants.[15] In the present calculations, the transferring hydrogen nucleus is treated classically, and the results are compared to experimental hydride transfer rates for the mutants measured at pH ≈ 7. For this reason, we

focus on the changes in the free energy barriers relative to the WT DHFR rather than the absolute free energy barriers.

The free energy barrier for each mutant is estimated by generating the potential of mean force for the hydride transfer reaction along a collective reaction coordinate using umbrella sampling techniques. The collective reaction coordinate is defined as the difference between the energies of the two VB states:

$$\Lambda(\mathbf{R})=V_{11}(\mathbf{R})-V_{22}(\mathbf{R}), \quad (1)$$

where $V_{11}(\mathbf{R})$ and $V_{22}(\mathbf{R})$ are the energies of VB states 1 and 2, respectively, and **R** denotes all nuclear coordinates. The molecular dynamics simulations are performed with mapping potentials defined as linear combinations of the energies of the two VB states:[7]

$$V_{\mathrm{map}}(\mathbf{R};\lambda_m)=(1-\lambda_m)V_{11}(\mathbf{R})+\lambda_m V_{22}(\mathbf{R}). \quad (2)$$

As the mapping parameter λ_m is varied from zero to unity, the reaction progresses from the reactant state to the product state. The potential of mean force is obtained by propagating a series of independent molecular dynamics simulations with different mapping potentials and combining them using the weighted histogram analysis method (WHAM)[47] or umbrella integration (UI).[5,6] The details of the molecular dynamics simulations[32] and the WHAM and UI implementations[8] are given elsewhere.

In our previous calculations of WT DHFR,[8] we used a set of 19 equally spaced windows with mapping parameters from λ_m = 0.05 to 0.95 with a spacing of 0.05. The starting configuration for each window was obtained from the previous window after 20 ps of equilibration. Each window was equilibrated for a total of 350 ps, followed by 300 ps of data collection. Using WHAM to generate the free energy profile from all of this data, we obtained a free energy barrier of 15.3 kcal/mol. This free energy barrier is within 0.5 kcal/mol of the values obtained from two other independent sets of data collected with a similar procedure[8] and is consistent with the free energy barrier of 15.4 kcal/mol obtained from another set of data generated using 20 mapping potentials with 4.5 ns of molecular dynamics for each window and an additional 2 ns for the four windows near the transition state (i.e., the top of the barrier).[32,45] All of these free energy barriers were obtained with a classical treatment of the transferring hydrogen nucleus.

In this paper, our objective is to estimate the free energy barriers for the mutants as efficiently as possible. Thus, we decreased the number of windows and the amount of equilibration and data collection for each window and confirmed that the desired accuracy for the free energy barrier is still maintained. For this purpose, we generated the free energy profile using WHAM with only six windows: λ_m = 0.050, 0.125, 0.250, 0.375, 0.500 and 0.625. These six windows enabled us to generate the portion of the free energy curve spanning the reactant and transition state regions, as required to calculate the free energy barrier for the forward hydride transfer reaction. As above, the starting configuration for each window was obtained from the previous window after 20 ps of equilibration. Each window was equilibrated for a total of 120 ps, followed by 250 ps of data collection. The resulting free energy barrier of 15.6 kcal/mol is similar to the 15.4 kcal/mol barrier obtained with 20 windows and significantly more equilibration and data collection.[32,45] When we analyzed the data using 70 ps of equilibration followed by 300 ps of data collection per window or, alternatively, 170 ps of equilibration followed by 200 ps of data collection per window, we obtained a free energy barrier of 15.7 kcal/mol or 15.6 kcal/mol, respectively. Thus, the free energy barrier is converged to within

0.3 kcal/mol using six windows and 120 ps of equilibration followed by 250 ps of data collection for each window.

Previously we showed that UI provides the same free energy profiles as WHAM but requires fewer windows for efficient convergence.[8] Using UI to generate the free energy profile, we obtained a free energy barrier of 15.4 kcal/mol with the six windows given above. We obtained a free energy barrier of 15.1 kcal/mol using only four of these windows: λ_m = 0.050, 0.250, 0.500 and 0.625. Based on this analysis, we compared the free energy barrier changes for the 15 mutants using WHAM with six windows and UI with both four and six windows. As will be shown below, the WHAM and UI methods with six windows lead to nearly identical results, and the UI method with four windows leads to qualitatively similar results with minor quantitative discrepancies.

The mutant structures of DHFR were generated from an equilibrated WT structure. The coordinates of this structure are given in Supporting Information. The profix utility in the JACKAL suite of programs[4,48] was used to generate the initial mutant structures from this WT structure. The profix utility uses a backbone rotamer library, a side-chain rotamer library, and distance geometry constraints to sample segment conformations. Missing residues are reconstructed with the Nest and Scap modules[4] in conjunction with the all-atom AMBER96 forcefield.[49] In our procedure, the coordinates of the residue to be mutated were deleted from the pdb file, the residue name was changed to the new name, and the profix utility was run for the modified pdb file. In addition to the mutated residue, the profix utility alters the conformations of neighboring residues until convergence.[4] For the DHFR mutants, we found that approximately four residues on each side of the mutation site were altered during this procedure.

The resulting mutant structures were subjected to four cycles of restrained minimizations and molecular dynamics simulations on the pure reactant potential energy surface with a gradual release of the atomic restraints. The initial restraining force constant on all atoms with respect to the initial structure was 59.75 kcal mol^{-1} $Å^{-2}$ and was halved with each cycle of the procedure. Each cycle consisted of a steepest descent geometry optimization followed by 15 ps of molecular dynamics. Subsequently, 650 ps of equilibration on the EVB reactant potential energy surface with λ_m = 0.05 was performed. After this equilibration, molecular dynamics simulations with mapping potentials corresponding to λ_m = 0.050, 0.125, 0.250, 0.375, 0.500 and 0.625 were propagated. The starting configuration for each window was obtained from the previous window after 20 ps of equilibration, and each window was equilibrated for a total of 120 ps, followed by 250 ps of data collection.

In order to confirm that the initial equilibration time of 650 ps on the EVB reactant surface was sufficient, we performed the calculations for all mutants with an initial equilibration time of only 300 ps on the EVB reactant surface. The free energy barriers differ from those obtained with 650 ps of equilibration by less than 0.5 kcal/mol for all mutants except G121P, G121V, D122A, and D27E. For these four mutants, we repeated the calculations with an initial equilibration time of 850 ps on the EVB reactant surface and found that the resulting free energy barriers are within 0.2 kcal/mol of those obtained with 650 ps of equilibration. Based on these tests, we conclude that an initial equilibration time of 650 ps on the EVB reactant potential energy surface is sufficient for all mutants studied.

The steps for calculating the free energy barrier change upon mutation, along with the approximate CPU times for a Xeon 3.0 GHz processor, are as follows:

1. Generation of mutant structure from WT using the profix utility (<2 CPU minutes)

2. Restrained minimizations/molecular dynamics on pure reactant surface (~8 CPU hours)
3. 650 ps equilibration on EVB reactant surface with λ_m = 0.05 (~65 CPU hours)
4. 120 ps equilibration and 250 ps data collection for each window (~37 CPU hours per window – the windows may be run in parallel on separate processors after the initial 20 ps per window)
5. Generation of free energy profiles using WHAM or UI (<2 CPU minutes)

This procedure is depicted in Figure 2. Note that this procedure does not include any free parameters or parameter fitting for the mutant calculations. The individual steps have been automated. For each mutant, the first three steps require only a single processor, and the fourth step can be run in parallel using four to six processors, depending on the number of windows used. Thus, the free energy barrier changes for 16 enzymes can be evaluated in approximately one week using 32 processors.

III. Results

Table 1 provides the experimentally determined rates for hydride transfer catalyzed by the 15 mutants. The locations of these mutation sites in the DHFR structure are depicted in Figure 3. Note that these mutation sites are distributed throughout the entire protein. The slowest mutant exhibits a decrease in the hydride transfer rate by a factor of ~1000, and the fastest mutant exhibits an increase in the hydride transfer rate by a factor of ~1.5. The associated experimental free energy barriers were obtained using the standard transition state theory rate constant expression, which neglects recrossings of the dividing surface. The effects of barrier recrossings can be included using a transmission coefficient prefactor. Previously the transmission coefficient was calculated to be close to unity for WT DHFR[31] and a mutant DHFR.[33] These previous results justify the neglect of barrier recrossing effects in the present study, which focuses on a qualitative ranking of mutant enzymes according to reaction rates. The experimentally measured hydride transfer rates depend on pH because of the accompanying proton transfer reaction. All of the experimental rates given in Table 1 were measured at pH 7 except for two mutants that were studied at pH 7.3. The difference between the hydride transfer rates for these two pH values is expected to be within the numerical accuracy of the computational methods. The experimental changes in the free energy barrier, $\Delta\Delta G^{\dagger}_{\text{expt}}$, are defined relative to the WT free energy barrier at pH 7.

Table 2 provides a comparison of the experimental and calculated changes in the free energy barrier relative to WT DHFR for the series of 15 mutants. The calculated changes in the free energy barrier are very similar using WHAM and UI with six windows. Figure 4 depicts a correlation plot of the results obtained using UI with six windows, in which case the correlation coefficient[50] is R = 0.82. The results obtained using UI with only four windows are qualitatively similar to those obtained using UI with six windows, but the quantitative changes in the free energy barrier differ by as much as 0.7 kcal/mol, and the correlation coefficient is R = 0.78. Given the significant approximations underlying the computational approach, this level of agreement between the calculated and experimental data is encouraging. Note that the computational approach predicts the correct direction of the change in free energy barrier for all 15 mutants.

While the objective of the present paper is to design, implement, and test an approach for ranking mutant enzymes according to the catalytic reaction rates, the data generated during this procedure could be used for further analysis of the impact of mutations. For this purpose, we have generated thermally averaged structures for the reactant and transition state windows (i.e., λ_m = 0.050 and 0.500). We have also calculated the thermally averaged hydride donor-

acceptor distances from these windows. We did not observe a strong correlation between these distances, or the differences between these distances, and the changes in the free energy barrier. Moreover, we did not observe a strong correlation between the proximity of the mutation site to the active site and the changes in the free energy barrier. Within the framework of our previous studies,[33,34,51] these results suggest that the mutations lead to nonlocal structural changes and changes in conformational motions of the entire enzyme that alter the relative probabilities of sampling transition state and reactant configurations, thereby altering the free energy barrier. Thus, these mutations impact the probability of sampling conformations conducive to the catalyzed chemical reaction, and even distal mutations far from the active site can significantly affect the reaction rate. A more detailed analysis of the thermally averaged structures and the conformational motions of the mutants is a direction for future research.

IV. Conclusions

In this paper, we presented a computationally efficient approach for evaluating the impact of mutation on enzyme-catalyzed reaction rates. This procedure requires the generation and equilibration of the mutant structure, followed by the calculation of a partial free energy curve using an empirical valence bond potential in conjunction with biased molecular dynamics simulations and umbrella integration. No parameter fitting is involved in this procedure for the mutants. The individual steps are automated and optimized for computational efficiency.

We used this approach to calculate the changes in the free energy barrier for hydride transfer upon mutation of DHFR. The 15 mutants studied were chosen objectively based on a general literature search for experimental measurements of the hydride transfer rate at pH 7.[44] The agreement between the calculated and experimental changes in the free energy barrier upon mutation is encouraging. The computational approach predicts the correct direction of the change in free energy barrier for all mutants, and the correlation coefficient between the calculated and experimental data is 0.82. In the future, this approach will be used to predict the impact of mutations that have not been studied experimentally yet. The feedback between experiment and theory will guide the further refinement of the procedure. This general approach for ranking protein designs according to the free energy barrier has implications for protein engineering and drug design.

Supplementary Material

Refer to Web version on PubMed Central for supplementary material.

Acknowledgements

We are grateful to Steve Benkovic for helpful discussions and to Jeeyeon Lee for compiling a list of DHFR mutants with the experimentally measured rate constants. We gratefully acknowledge Dhruva Chakravorty for his assistance in calculating the thermally averaged structures for the mutants. We are also thankful for financial support from the National Institutes of Health (NIH) grant GM56207 and the Defense Advanced Research Projects Agency (DARPA).

References

1. Rothlisberger D, Khersonsky O, Wollacott AM, Jiang L, DeChancie J, Betker J, Gallaher JL, Althoff EA, Zanghellini A, Dym O, Albeck S, Houk KN, Tawfik DS, Baker D. Nature (London) 2008;453:190. [PubMed: 18354394]
2. Jiang L, Althoff EA, Clemente FR, Doyle L, Rothlisberger D, Zanghellini A, Gallaher JL, Betker JL, Tanaka F, Barbas CF III, Hilvert D, Houk KN, Stoddard BL, Baker D. Science 2008;319:1387. [PubMed: 18323453]
3. Das R, Baker D. Annu Rev Biochem 2008;77:363. [PubMed: 18410248]
4. Xiang Z, Honig B. J Mol Biol 2001;311:421. [PubMed: 11478870]

5. Kastner J, Thiel W. J Chem Phys 2005;123:144104. [PubMed: 16238371]
6. Kastner J, Thiel W. J Chem Phys 2006;124:234106. [PubMed: 16821906]
7. Warshel, A. Computer Modeling of Chemical Reactions in Enzymes and Solutions. John Wiley & Sons, Inc.; New York: 1991.
8. Chakravorty DK, Kumarasiri M, Soudackov AV, Hammes-Schiffer S. Journal of Chemical Theory and Computation 2008;4:1974. [PubMed: 19319209]
9. Miller GP, Benkovic SJ. Chemistry & Biology 1998;5:R105. [PubMed: 9578637]
10. Berg, JM.; Stryer, L.; Tymoczko, J. Biochemistry. Vol. 5th ed. Freeman: New York; 2002.
11. Miovic M, Pizer LI. Journal of Bacteriology 1971;106:856. [PubMed: 4254117]
12. Allegra CJ, Hoang K, Yeh GC, Drake JC, Baram J. J Biol Chem 1987;262:13520. [PubMed: 2443493]
13. Huennekens FM. Advances in Enzyme Regulation 1994;34:397. [PubMed: 7942284]
14. Schweitzer BI, Dicker AP, Bertino JR. FASEB J 1990;4:2441. [PubMed: 2185970]
15. Fierke CA, Johnson KA, Benkovic SJ. Biochemistry 1987;26:4085. [PubMed: 3307916]
16. Cameron CE, Benkovic SJ. Biochemistry 1997;36:15792. [PubMed: 9398309]
17. David CL, Howell EE, Farnum MF, Villafranca JE, Oatley SJ, Kraut J. Biochemistry 1992;31:9813. [PubMed: 1356437]
18. Rajagopalan PTR, Lutz S, Benkovic SJ. Biochemistry 2002;41:12618. [PubMed: 12379104]
19. Miller GP, Benkovic SJ. Biochemistry 1998;37:6336. [PubMed: 9572848]
20. Adams JA, Fierke CA, Benkovic SJ. Biochemistry 1991;30:11046. [PubMed: 1834173]
21. Miller GP, Wahnon DC, Benkovic SJ. Biochemistry 2001;40:867. [PubMed: 11170407]
22. Sawaya MR, Kraut J. Biochemistry 1997;36:586. [PubMed: 9012674]
23. Osborne MJ, Schnell J, Benkovic SJ, Dyson HJ, Wright PE. Biochemistry 2001;40:9846. [PubMed: 11502178]
24. Schnell JR, Dyson HJ, Wright PE. Annual Review of Biophysical Biomolecular Structure 2004;33:119.
25. Zhang ZQ, Rajagopalan PTR, Selzer T, Benkovic SJ, Hammes GG. Proc Nat Acad Sci USA 2004;101:2764. [PubMed: 14978269]
26. Sikorski RS, Wang L, Markham KA, Rajagopalan PTR, Benkovic SJ, Kohen A. J Am Chem Soc 2004;126:4778. [PubMed: 15080672]
27. Antikainen NM, Smiley RD, Benkovic SJ, Hammes GG. Biochemistry 2005;44:16835. [PubMed: 16363797]
28. Wang L, Goodey NM, Benkovic SJ, Kohen A. Proceedings of the National Academy of Sciences USA 2006;103:15753.
29. Boehr DD, McElheny D, Dyson HJ, Wright PE. Science 2006;313:1638. [PubMed: 16973882]
30. Agarwal PK, Billeter SR, Rajagopalan PTR, Benkovic SJ, Hammes-Schiffer S. Proc Natl Acad Sci USA 2002;99:2794. [PubMed: 11867722]
31. Agarwal PK, Billeter SR, Hammes-Schiffer S. J Phys Chem B 2002;106:3283.
32. Wong KF, Watney JB, Hammes-Schiffer S. J Phys Chem B 2004;108:12231.
33. Watney JB, Agarwal PK, Hammes-Schiffer S. J Am Chem Soc 2003;125:3745. [PubMed: 12656604]
34. Wong KF, Selzer T, Benkovic SJ, Hammes-Schiffer S. Proc Natl Acad Sci USA 2005;102:6807. [PubMed: 15811945]
35. Castillo R, Andres J, Moliner V. J Am Chem Soc 1999;121:12140.
36. Radkiewicz JL, Brooks CL III. J Am Chem Soc 2000;122:225.
37. Cummins PL, Greatbanks SP, Rendell AP, Gready JE. J Phys Chem B 2002;106:9934.
38. Garcia-Viloca M, Truhlar DG, Gao J. Biochemistry 2003;42:13558. [PubMed: 14622003]
39. Rod TH, Radkiewicz JL, Brooks CL III. Proceedings of the National Academy USA 2003;100:6980.
40. Thorpe IF, Brooks CL III. J Phys Chem B 2003;107:14042.
41. Thorpe IF, Brooks CL III. Proteins: Structure, Function, and Bioinformatics 2004;57:444.
42. Swanwick RS, Shrimpton PJ, Allemann RK. Biochemistry 2004;43:4119. [PubMed: 15065854]
43. Liu H, Warshel A. Biochemistry 2007;46:6011. [PubMed: 17469852]

44. Lee, J.; Benkovic, SJ. personal communication
45. Wang Q, Hammes-Schiffer S. J Chem Phys 2006;125:184102. [PubMed: 17115733]
46. van Gunsteren, WF.; Billeter, SR.; Eising, AA.; Hunenberger, PH.; Kruger, P.; Mark, AE.; Scott, WRP.; Tironi, IG. Biomolecular simulation: The GROMOS96 manual and user guide. VdF Hochschulverlag, ETH Zurich; Zurich: 1996.
47. Kumar S, Rosenberg JM, Bouzida D, Swendsen RH, Kollman PA. J Comput Chem 1992;13:1011.
48. Xiang, JZ.; Honig, B. JACKAL: A Protein Structure Modeling Package. Columbia University & Howard Hughes Medical Institute; New York: 2002.
49. Cornell WD, Cieplak P, Bayly CI, Gould IR, Merz KM Jr, Ferguson DM, Spellmeyer DC, Fox T, Caldwell JW, Kollman PA. J Am Chem Soc 1995;117:5179.
50. Weisstein, EW. “Correlation Coefficient” From MathWorld - A Wolfram Web Resource. http://mathworld.wolfram.com/CorrelationCoefficient.html
51. Benkovic SJ, Hammes GG, Hammes-Schiffer S. Biochemistry 2008;47:3317. [PubMed: 18298083]

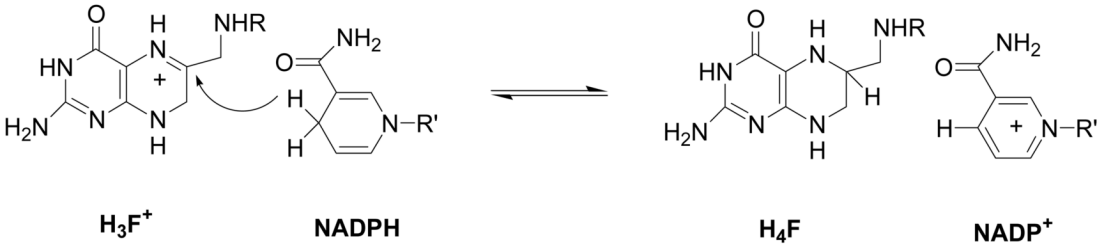

Figure 1.
Hydride transfer reaction from the NADPH cofactor to the protonated dihydrofolate substrate H_3F^+ to form the products tetrahydrofolate H_4F and $NADP^+$. Figure reproduced with permission from Ref. 8.

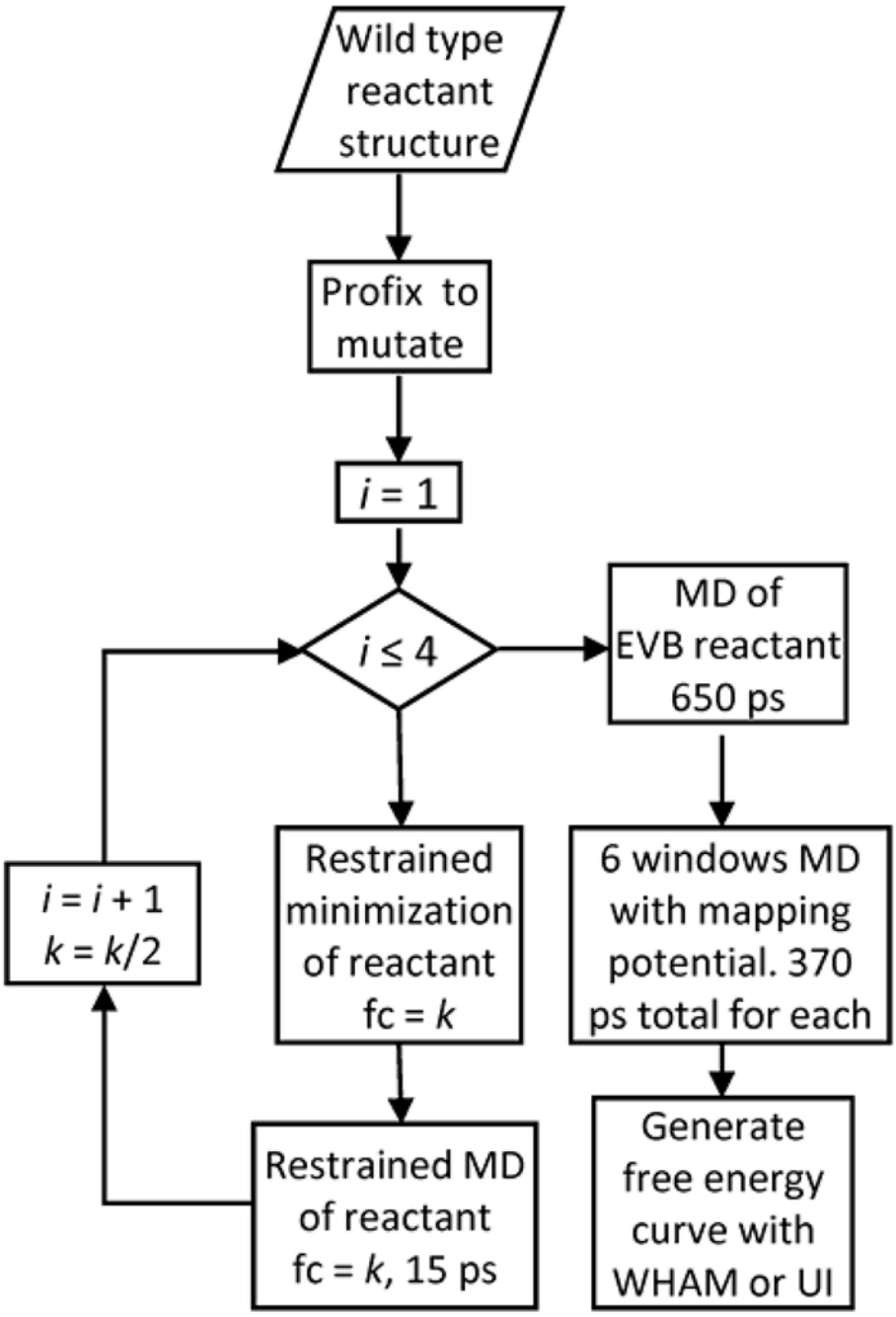

Figure 2.
Summary of the steps for the generation of the initial mutant structure, equilibration, and calculation of the free energy barrier. Here fc is the force constant of the position restraints with respect to the initial structure during the restrained minimizations and molecular dynamics simulations.

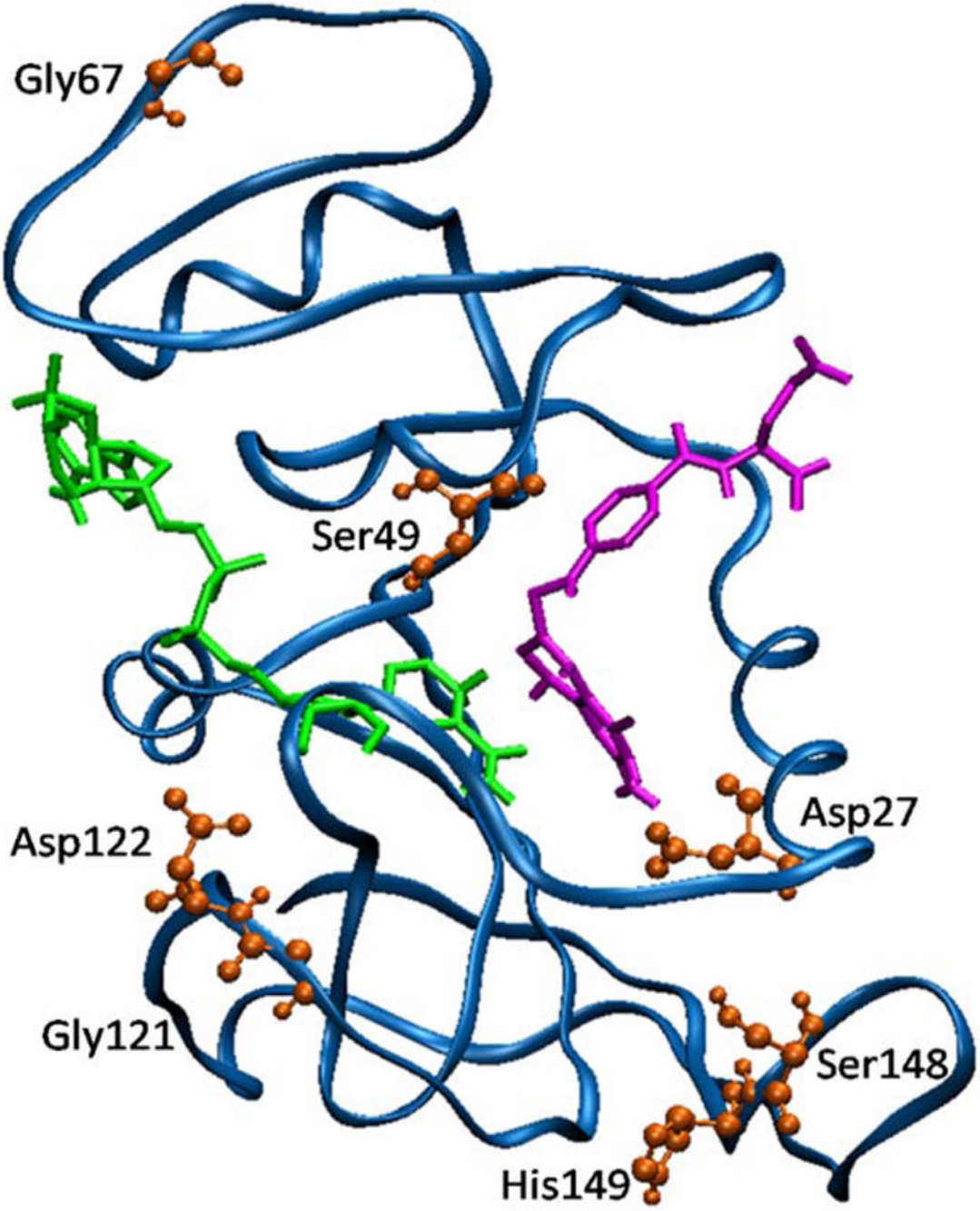

Figure 3.
Depiction of the mutation sites of DHFR. The cofactor is green, the substrate is magenta, and the mutated residues are red.

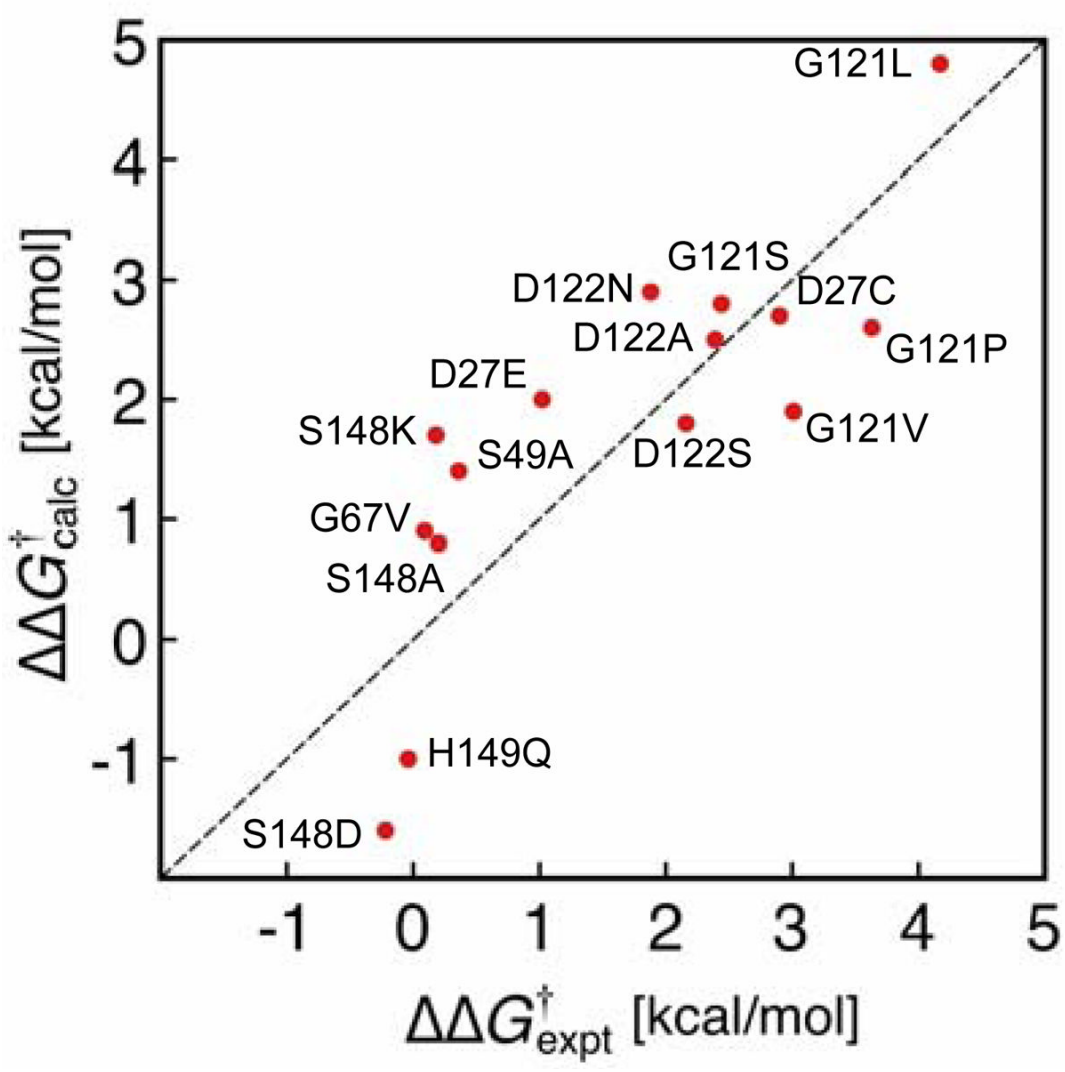

Figure 4.

Correlation plot for the calculated and experimental changes in the free energy barrier for the 15 mutants, where the calculated free energy barriers were obtained using UI with six windows. The correlation coefficient is $R = 0.82$. The diagonal dashed line corresponding to $\Delta\Delta G^{\dagger}_{\text{expt}} = \Delta\Delta G^{\dagger}_{\text{calc}}$ is provided for visual guidance.

Table 1

The experimentally determined hydride transfer rate constants for *E. coli* DHFR mutants at 300 K. These rate constants were measured at pH 7 for WT DHFR and all mutants except D27E and D27C, which were measured at pH 7.3.

Mutant	k_{hyd} (s^{-1})
G121L[16]	0.2
G121P[16]	0.5
G121V[16]	1.4
D27C[17]	1.7
G121S[18]	3.7
D122A[19]	4.0
D122S[19]	5.9
D122N[19]	9.4
D27E[17]	40
S49A[20]	120
S148A[21]	157
S148K[21]	162
G67V[18]	190
WT[16]	220
H149Q[44]	234
S148D[21]	319

Table 2

The change in the free energy barrier relative to the WT free energy barrier for a series of mutants. The experimental free energy barriers are obtained from the transition state theory rate constant expression $k=\frac{k_B T}{h}\exp(-\Delta G^{\dagger}/k_B T)$ using the experimentally determined rate constants in Table 1. The calculated free energy barriers are obtained using WHAM with six windows, UI with six windows, and UI with four windows. All free energies are given in kcal/mol.

Mutant	$\Delta\Delta G^{\dagger}_{expt}$	$\Delta\Delta G^{\dagger}_{calc}$ WHAM	$\Delta\Delta G^{\dagger}_{calc}$ UI6	$\Delta\Delta G^{\dagger}_{calc}$ UI4
G121L	4.2	4.3	4.8	4.4
G121P	3.6	2.2	2.6	3.0
G121V	3.0	1.6	1.9	2.4
D27C	2.9	2.6	2.7	2.9
G121S	2.4	2.4	2.8	3.3
D122A	2.4	2.3	2.5	2.9
D122S	2.2	1.6	1.8	2.2
D122N	1.9	2.8	2.9	3.4
D27E	1.0	1.9	2.0	2.6
S49A	0.36	1.2	1.4	1.8
S148A	0.20	0.4	0.8	1.5
S148K	0.18	1.7	1.7	2.0
G67V	0.09	0.9	0.9	1.6
H149Q	−0.04	−1.3	−1.0	−1.0
S148D	−0.22	−1.6	−1.6	−0.9